

# Modeling and simulation of the post-impact trajectories of particles in oblique precision shot-peening

T. I. Zohdi<sup>1</sup>

Received: 8 April 2015 / Revised: 15 May 2015 / Accepted: 19 May 2015  
© OWZ 2015

**Abstract** The use of targeted particulate jets for surface modification in advanced manufacturing processes such as shot-peening are now becoming widespread. The degree of precision now demanded, in tightly confined workspaces, dictates that these processes undergo deeper scrutiny, refinement and optimization, in particular to avoid unintended excessive normal and tangential impact forces and re-impact from the rebounding jet on secondary surfaces. This work focuses on the building block of a particulate jet, namely the inelastic impact of a particle with a surface. The governing equations for a general three-dimensional inelastic impact with unilateral stick-slip conditions are derived, with the objective being to extract the particle and target characteristics which control the forces induced on impact and the resulting post-impact trajectories. Quantitative and qualitative analyses are performed for different types of surfaces and allows analysts to make informed decisions on the choices of parameters in jets, in order to reduce trial and error procedures.

**Keywords** Shot-peening · Particulate jets · Impact

## 1 Introduction

Standard shot peening is a cold-working process whereby smooth hard spheres are projected at surfaces in order to induce compressive stresses, upon impact, in the surface and near surface of industrial components, such as turbine blades, gears, cam shafts, etc. The objective is to suppress failure

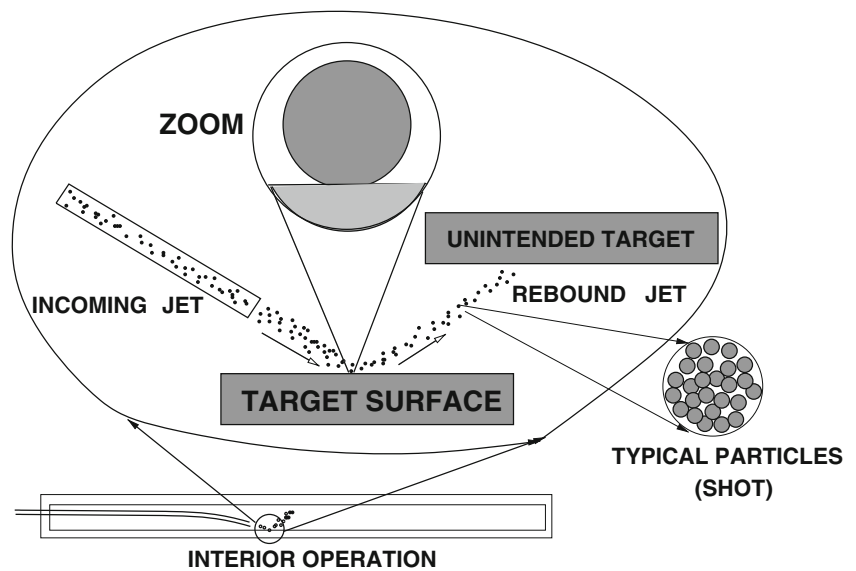
mechanisms, which are usually driven by tensile stresses, such as crack propagation and fatigue, by preemptively placing the surface in a state of compression. The main idea in shot peening is that the stresses underneath the shot will exceed the plastic yield strain, thus causing the surface material to stretch radially from the center of the contact zone. When the shot loses contact, the material recovers, and is in compression, due to the surrounding material pressing against the plastified (surface stretched) material. Smooth hard balls (“shot”) are used, since they usually do not break because of their hardened spherical exterior, thus producing no sharp edges. This also allows the shot particles to be re-used repeatedly. The smooth exterior also allows for minimum gouging, which can initiate cracks. The shot is usually made by cutting wrought carbon steel wire, and rolling the bits into spherical shot. Often, stainless steel is used, if carbon contamination is an issue. Furthermore, if iron contamination is a concern, then glass beads are used.

Currently, an emerging process of technological importance is precise, targeted, shot-peening applied deep within interior keyways and pathways inside complex machine components, such as cylinder blocks, turbines, fan blades and compressors, which are expected to undergo harsh industrial environments. Furthermore, new small-scale devices, with extremely complex topologies (Dirksen et al [8], Lum et al [14]), which are expected to undergo cyclical loading, are potential applications for precise, targeted, shot-peening. Typically, these approaches utilize long needle-like nozzles to deliver the shot-peening particles (Fig. 1). In most cases, the impact will be oblique (not perpendicular to the surface). Thus, as shot-peening technology continues to be applied to smaller and more confined spaces, impacts may have to be delivered with an angular jet. Thus, questions naturally arise in the performance of these approaches, as a function of the characteristics of the jet particles and the surface of

✉ T. I. Zohdi  
zohdi@berkeley.edu

<sup>1</sup> Department of Mechanical Engineering, University of California, Berkeley, CA 94720-1740, USA

**Fig. 1** A particulate shot-peening jet applied to a target surface and potential rebound with unintended surfaces



the target. In particular, one would like to avoid unintended excessive normal and tangential impact forces and re-impact from the rebounding jet on secondary surfaces. It is important to determine the imparted impact forces on the target surface since, while shot-peening is desired to mitigate cracking, fatigue failure, etc, over-peening can actually enhance failure by inducing highly localized stress concentrations. In some cases, large tangential friction forces induced during oblique impact can lead to surface spall, thus actually ablating the surface. Accordingly, this work focusses on the building block of a particulate shot-peening jet, namely the oblique inelastic impact of a particle with a frictional surface. Specifically, the governing equations for a general three-dimensional inelastic impact with unilateral stick-slip conditions are derived, with the objective being to determine the relationship between pre- and post-impact particle trajectory and the imparted forces on the surface. The analysis is useful to researchers in the field interested in the analysis of particulate machining jets, in order to reduce trial and error procedures.

*Remarks* We note that the deformation and stress analysis of an impacted surface, which is an extremely complex process, is outside the scope of the current study. For a modern, in depth, analysis of the modeling and simulation of the deformation of contacting bodies, we refer the reader to Wriggers [21]. We also refer the reader to Afazov et al [1], Bagherifard et al [3], Elbella et al [10] and Chen et al [7] for the finite element analysis of the response of the substrate of a shot-peened solid and recently to Zohdi [25] for rapid computation of multiple contacting bodies on substrates for additive particle printing processes. It is important to note that for more complex cases involving heat generation, the deformation of the contacting surfaces and potentially other mutliphysical phenomena can be handled using numerical algorithms based on methods found in the treatise of Wriggers [21]. For mul-

tipple bodies in simultaneous contact, numerical schemes are needed for contact detection, stick-slip checks, etc., which are discussed in the conclusions of this work.

## 2 General impact, spin and sliding

We formulate a three-dimensional impact scenario as shown in Fig. 2. The formulation is capable of describing impact cases of a particle with incoming spin. We assume that the target surface, which is massive relative to the particle, does not move.

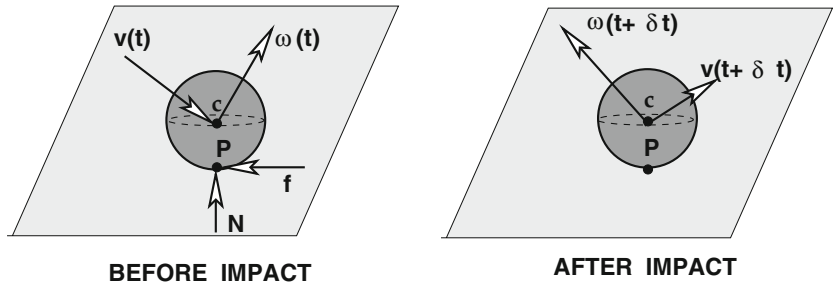
The impulse in the normal direction for the center of mass, located at point  $c$ , is governed by a balance of linear momentum in the normal ( $e_n$ ) direction<sup>1</sup>

$$mv_{c,n}(t) + N\delta t = mv_{c,n}(t + \delta t) \\ \Rightarrow N = m \frac{(v_{c,n}(t + \delta t) - v_{c,n}(t))}{\delta t}, \quad (1)$$

where  $m$  is the mass of the particle,  $v_{c,n}(t)$  is the normal component of the velocity of point  $c$  before impact,  $N$  is the normal contact force,  $\delta t$  is the impact duration time and  $v_{c,n}(t + \delta t)$  is the normal component of the velocity of point  $c$  after impact. A balance of momentum along the direction of the induced friction force provides a means by which one

<sup>1</sup> We ignore gravity throughout the analysis. Furthermore, we will ignore any aerodynamic effects, such as drag and the Magnus effect, whereby a spinning particle with angular velocity  $\omega$  and velocity  $v_c$  creates unequal drag forces on the surface, since the points on the surface are traveling at unequal absolute speeds ( $v_p = v_c + \omega \times r_{c \rightarrow p}$ ). We concentrate only on the instants directly before and after the impact event itself.

**Fig. 2** A 3-D view of an inelastic pre- and post-impact of a particle on a surface



can compute the friction force

$$mv_{c,t}(t) + f\delta t = mv_{c,t}(t + \delta t) \Rightarrow f = m \frac{(v_{c,t}(t + \delta t) - v_{c,t}(t))}{\delta t}, \tag{2}$$

where  $v_{c,t}(t)$  is the tangential component of the velocity of point  $c$  before impact,  $f$  is the friction contact force and  $v_{c,t}(t + \delta t)$  is the tangential component of the velocity of point  $c$  after impact. The direction of the line of action is given by the initial relative tangential velocity at point  $p$

$$\mathbf{e}_t = \frac{\mathbf{v}_{p,t}(t)}{\|\mathbf{v}_{p,t}(t)\|}, \tag{3}$$

where the tangential velocity of the particle is

$$\mathbf{v}_{p,t}(t) = \mathbf{v}_p(t) - (\mathbf{v}_p(t) \cdot \mathbf{e}_n(t))\mathbf{e}_n. \tag{4}$$

We note that  $\mathbf{e}_n$  is invariant for a sphere and plane, and we assume that  $\mathbf{e}_t$  is the tangent vector during the impact event. If the particle slips, then direction of friction is

$$\mathbf{f} = -f\mathbf{e}_t. \tag{5}$$

The velocities of points  $c$  and  $p$  are related by

$$\mathbf{v}_c = \mathbf{v}_p + \boldsymbol{\omega} \times \mathbf{r}_{p \rightarrow c} \Rightarrow \mathbf{v}_p = \mathbf{v}_c + \boldsymbol{\omega} \times \mathbf{r}_{c \rightarrow p}, \tag{6}$$

where  $\|\mathbf{r}_{p \rightarrow c}\| = \|\mathbf{r}_{c \rightarrow p}\| = R$  is the sphere radius. We employ a normal coefficient of restitution that provides information on the velocities of surfaces before and after impact, in the normal direction between the contact point  $p$  and the surface:<sup>2</sup>

$$\mathcal{E} = \frac{v_{p,n}(t + \delta t) - 0}{0 - v_{p,n}(t)}, \tag{7}$$

where  $0 \leq \mathcal{E} \leq 1$ . Thus,

$$v_{p,n}(t + \delta t) = -\mathcal{E}v_{p,n}(t). \tag{8}$$

<sup>2</sup> If one assumed that the surface's velocity was zero, we would obtain  $v_{p,n}(t + \delta t) = -v_{p,n}(t)\mathcal{E}$ .

Also, the normal components of  $p$  and  $c$  are related by

$$v_{p,n} = \mathbf{v}_p \cdot \mathbf{e}_n = (\mathbf{v}_c + \boldsymbol{\omega} \times \mathbf{r}_{c \rightarrow p}) \cdot \mathbf{e}_n = v_{c,n}, \tag{9}$$

where  $\mathbf{e}_n$  is the unit vector in the normal direction. Thus,  $v_{c,n}(t + \delta t) = v_{p,n}(t + \delta t)$  and the normal force becomes

$$N = m \frac{v_{c,n}(t + \delta t) - v_{c,n}(t)}{\delta t} = -mv_{c,n}(t) \frac{(1 + \mathcal{E})}{\delta t}. \tag{10}$$

The tangential components are related by

$$v_{p,t} = \mathbf{v}_p \cdot \mathbf{e}_t = (\mathbf{v}_c + \boldsymbol{\omega} \times \mathbf{r}_{c \rightarrow p}) \cdot \mathbf{e}_t = v_{c,t} + (\boldsymbol{\omega} \times \mathbf{r}_{c \rightarrow p}) \cdot \mathbf{e}_t \tag{11}$$

where  $\mathbf{e}_t$  is the unit vector in the tangential direction. Thus,

$$v_{c,t}(t + \delta t) = v_{p,t}(t + \delta t) - (\boldsymbol{\omega}(t + \delta t) \times \mathbf{r}_{c \rightarrow p}) \cdot \mathbf{e}_t. \tag{12}$$

An orthogonal direction to the plane of normal and friction forces is given by

$$\mathbf{e}_o = \mathbf{e}_t \times \mathbf{e}_n \tag{13}$$

and since there are no forces acting in that direction during impact, the velocity components in that direction remain unchanged

$$v_c(t) \cdot \mathbf{e}_o = v_c(t + \delta t) \cdot \mathbf{e}_o. \tag{14}$$

The total velocity of point  $c$  is given by summing the velocities in the three orthogonal directions

$$\mathbf{v}_c(t + \delta t) = v_{c,t}(t + \delta t)\mathbf{e}_t + v_{c,n}(t + \delta t)\mathbf{e}_n + v_{c,o}(t + \delta t)\mathbf{e}_o. \tag{15}$$

### 2.1 Stick-slip friction

Using the preceding relations, the friction force is thus given by

$$f = m \left( \frac{(v_{p,t}(t + \delta t) - (\boldsymbol{\omega}(t + \delta t) \times \mathbf{r}_{c \rightarrow p}) \cdot \mathbf{e}_t) - v_{c,t}(t))}{\delta t} \right) \quad (16)$$

Computing the angular momentum about point  $c$ , yields  $\boldsymbol{\omega}(t + \delta t)$

$$\bar{\mathbf{I}} \cdot \boldsymbol{\omega}(t) + \mathbf{r}_{c \rightarrow p} \times \mathbf{f} \delta t = \bar{\mathbf{I}} \cdot \boldsymbol{\omega}(t + \delta t) \Rightarrow \boldsymbol{\omega}(t + \delta t) = \boldsymbol{\omega}(t) + \frac{(\mathbf{r}_{c \rightarrow p} \times \mathbf{f}) \delta t}{\bar{\mathbf{I}}}, \quad (17)$$

where  $\bar{\mathbf{I}} = \bar{I} \mathbf{1}$ , where  $\bar{I} = \frac{2}{5} m R^2$  for a solid sphere. Substituting Eq. 16 into Eq. 17 yields the following for the friction force

$$f = - \frac{m \bar{I}}{\delta t (\bar{I} + m R^2)} \times (v_{p,t}(t + \delta t) - (\boldsymbol{\omega}(t) \times \mathbf{r}_{c \rightarrow p}) \cdot \mathbf{e}_t - v_{c,t}(t)). \quad (18)$$

We must subsequently check two cases: (1) tangential stick and (2) possible slip.

### 2.2 Case 1: no tangential slip

If we assume no tangential slip, thus  $v_{pt}(t + \delta t) = 0$ , leading to

$$f = \frac{m \bar{I}}{\delta t (\bar{I} + m R^2)} ((\boldsymbol{\omega}(t) \times \mathbf{r}_{c \rightarrow p}) \cdot \mathbf{e}_t + v_{c,t}(t)), \quad (19)$$

where  $N = - \frac{m v_{c,n}(t)}{\delta t} (1 + \mathcal{E})$ , where

$$\boldsymbol{\omega}(t + \delta t) = \boldsymbol{\omega}(t) + \frac{(\mathbf{r}_{c \rightarrow p} \times \mathbf{f}) \delta t}{\bar{\mathbf{I}}} = \boldsymbol{\omega}(t) - \frac{f R \delta t}{\bar{\mathbf{I}}} \mathbf{e}_o, \quad (20)$$

and

$$v_{c,t}(t + \delta t) = v_{c,t}(t) - \frac{f \delta t}{m} \quad (21)$$

Slipping occurs if the Coulomb friction limit is exceeded.

### 2.3 Case 2: slipping

If the Coulomb friction limit is exceeded

$$|f| > \mu_s |N|, \quad (22)$$

this implies that the no slip assumption is incorrect, then

$$\mathbf{f} = -\mu_d N \mathbf{e}_t = \frac{m \mu_d}{\delta t} (1 + \mathcal{E}) v_{c,n}(t) \mathbf{e}_t, \quad (23)$$

where we note that  $v_{c,n}(t)$  is negative. Thus,

$$\begin{aligned} \boldsymbol{\omega}(t + \delta t) &= \boldsymbol{\omega}(t) + \frac{(\mathbf{r}_{c \rightarrow p} \times \mathbf{f}) \delta t}{\bar{\mathbf{I}}} = \boldsymbol{\omega}(t) - \frac{\mu_d N R \delta t}{\bar{\mathbf{I}}} \mathbf{e}_o \\ &= \boldsymbol{\omega}(t) + \frac{m \mu_d (1 + \mathcal{E}) v_{c,n}(t) R}{\bar{\mathbf{I}}} \mathbf{e}_o, \end{aligned} \quad (24)$$

and

$$\begin{aligned} v_{c,t}(t + \delta t) &= v_{c,t}(t) - \frac{f \delta t}{m} = v_{c,t}(t) - \frac{\mu_d N \delta t}{m} \\ &= v_{c,t}(t) - \mu_d (1 + \mathcal{E}) v_{c,n}(t) \end{aligned} \quad (25)$$

*Remark 1* In order to determine post impact trajectories, which are needed to determine the tool path and to protect against unintended damage, one can post process the post-impact velocity vector and unit vector ( $\mathbf{d}(t + \delta t)$ ):

$$\mathbf{d}(t + \delta t) \stackrel{\text{def}}{=} \frac{\mathbf{v}(t + \delta t)}{\|\mathbf{v}(t + \delta t)\|}. \quad (26)$$

*Remark 2* We note that the time-averaged impulses

$$N^* \stackrel{\text{def}}{=} N \delta t \quad (27)$$

and

$$f^* \stackrel{\text{def}}{=} f \delta t, \quad (28)$$

which are two of the primary quantities of interest, are independent of  $\delta t$ .

### 2.4 Special cases: purely planar jet impact

In the case of purely planar impact, with  $\boldsymbol{\omega}(t) = \omega(t) \mathbf{e}_o$ , the two previous cases simplify even further (Fig. 3).

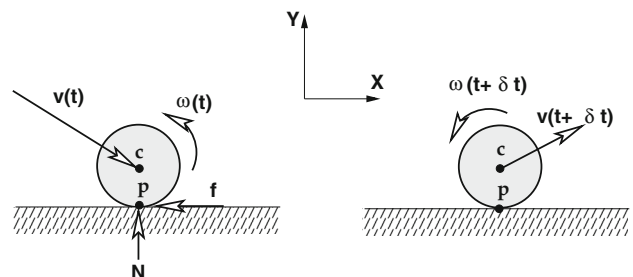


**Fig. 3** Purely planar impact scenario

### 2.4.1 Case 1: no tangential slip

If we assume no tangential slip, thus  $v_{pt}(t + \delta t) = 0$ , leading to

$$f = \frac{m\bar{I}}{\delta t(\bar{I} + mR^2)} (\omega(t)R + v_{c,t}(t)), \tag{29}$$

where  $N = -\frac{mv_{c,n}(t)}{\delta t}(1 + \mathcal{E})$ , and

$$\omega(t + \delta t) = \omega(t) - \left(\frac{mR}{\bar{I} + mR^2}\right) (\omega(t)R + v_{c,t}(t)) \tag{30}$$

and

$$v_{c,t}(t + \delta t) = v_{c,t}(t) - \left(\frac{\bar{I}}{\bar{I} + mR^2}\right) (\omega(t)R + v_{c,t}(t)) \tag{31}$$

and, as before

$$v_{c,n}(t + \delta t) = -\mathcal{E}v_{c,n}(t). \tag{32}$$

### 2.5 Case 2: slipping

As before, if the Coulomb friction limit is exceeded, this implies that the no slip assumption is incorrect, then friction acts in the opposite  $e_t$  direction with magnitude

$$f = \mu_d N = -\frac{m\mu_d}{\delta t}(1 + \mathcal{E})v_{c,n}(t), \tag{33}$$

where we note that  $v_{c,n}(t)$  is negative, and

$$\omega(t + \delta t) = \omega(t) + \frac{m\mu_d(1 + \mathcal{E})v_{c,n}(t)R}{\bar{I}}, \tag{34}$$

and

$$v_{c,t}(t + \delta t) = v_{c,t}(t) - \frac{\mu_d N \delta t}{m} = v_{c,t}(t) - \mu_d(1 + \mathcal{E})v_{c,n}(t) \tag{35}$$

and, as before

$$v_{c,n}(t + \delta t) = -\mathcal{E}v_{c,n}(t). \tag{36}$$

*Remark* In either case, the trajectory of the post-impact angle is

$$\theta(t + \delta t) = \tan^{-1} \left( \frac{v_{c,n}(t + \delta t)}{v_{c,t}(t + \delta t)} \right), \tag{37}$$

and since  $v_{c,t}(t + \delta t)$  will generally decrease for greater friction, a more vertical trajectory occurs.

*Remark* One could consider models that are irrotational, which could be applicable to problems of ablation or surface deposition. If we constrain the shot-sphere to behave as an irrotational particle, we have simplified versions of (1) tangential stick and (2) possible slip:

- **Case 1-no tangential slip:** If we assume no tangential slip, thus  $v_{pt}(t + \delta t) = v_{c,t}(t + \delta t) = 0$ , leading to

$$f = \frac{mv_{c,n}(t)}{\delta t} \tag{38}$$

where, as before,  $N = -\frac{mv_{c,n}(t)}{\delta t}(1 + \mathcal{E})$ , and

$$v_{c,n}(t + \delta t) = -\mathcal{E}v_{c,n}(t). \tag{39}$$

- **Case 2-Slipping:** As before, if the Coulomb friction limit is exceeded, this implies that the no slip assumption is incorrect, then friction acts in the opposite  $e_t$  direction with magnitude

$$f = \mu_d N = -\frac{m\mu_d}{\delta t}(1 + \mathcal{E})v_{c,n}(t), \tag{40}$$

where we note that  $v_{c,n}(t)$  is negative, and

$$\omega(t + \delta t) = \omega(t) + \frac{m\mu_d(1 + \mathcal{E})v_{c,n}(t)R}{\bar{I}}, \tag{41}$$

and

$$\begin{aligned} mv_{c,t}(t) + f &= mv_{c,t}(t + \delta t) \Rightarrow v_{c,t}(t + \delta t) \\ &= v_{c,t}(t) - \mu_d(1 + \mathcal{E})v_{c,n}(t) \end{aligned} \tag{42}$$

and, as before

$$v_{c,n}(t + \delta t) = -\mathcal{E}v_{c,n}(t). \tag{43}$$

In either case, the trajectory of the post-impact angle is

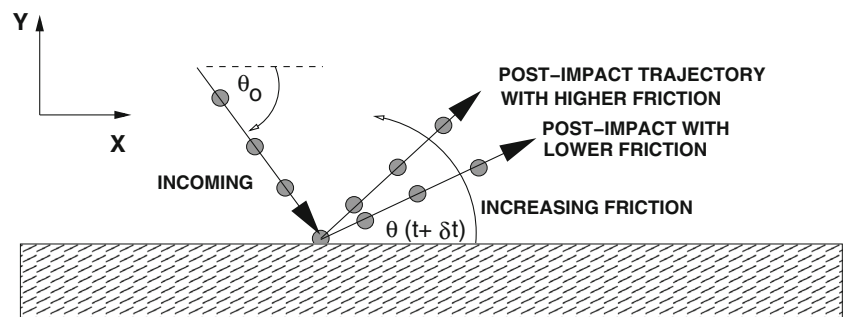
$$\theta(t + \delta t) = \tan^{-1} \left( \frac{v_{c,n}(t + \delta t)}{v_{c,t}(t + \delta t)} \right), \tag{44}$$

however, in the no slip case,  $\theta = \frac{\pi}{2}$ , which is purely vertical, and in the slipping case,

$$\theta(t + \delta t) = \tan^{-1} \left( \frac{-\mathcal{E}v_{c,n}(t)}{v_{c,t}(t) + \mu_d(1 + \mathcal{E})v_{c,n}(t)} \right), \tag{45}$$

which implies for greater friction, a more vertical trajectory occurs.

**Fig. 4** Impact trajectories with varying friction



### 3 Realistic parameters for shot peening particles

The following system parameters are considered, corresponding closely to that of a small-scale shot-peening particle:

- Sphere radius:  $R = 0.0005$  m,
- Density of the sphere:  $\rho_p = 7000 \text{ kg/m}^3$ , thus the mass is  $m_p = \frac{4}{3}\pi R^3$ ,
- Initial velocity of the sphere:  $\mathbf{v}(t = 0) = (v_{xo}, v_{yo}, v_{zo}) = v_o(\cos(\theta_o), -\sin(\theta_o), 0)$ , where  $v_o = 10$  m/sec and  $\theta_o = \frac{\pi}{3}$ ,
- Initial angular velocity of the sphere:  $\boldsymbol{\omega} = (\omega_{xo}, \omega_{yo}, \omega_{zo}) = (0, 0, 0)$  rad/sec,
- Static friction coefficient:  $0 \leq \mu_s \leq 0.3$  and a dynamic friction coefficient:  $\mu_d = 0.9\mu_s$ ,
- Normal coefficient of restitution:  $\mathcal{E} = 0.25$ .

The differences in the trajectory of a post-impact particle are substantial with varying friction. As Table 1 illustrates, with increasing friction the trajectory increases (steeper rebound relative to the impact plane). Table 2 illustrates the imparted force-impulses and translational and rotational kinetic energies. In all cases there was tangential slipping. The subsequent post-impact spin is also substantial due to the “jolt” from friction, combined with the fact that the particles are small. With increasing friction, more translational kinetic energy is converted into rotational energy. The last column of Table 2 illustrates that there is value of  $\mu_s$  (and  $\mu_d = 0.9\mu_s$ ) for which the energy lost is maximized (post-impact energy minimized to 22.5% of the original). This occurs at approximately  $\mu_s = 0.15$  for the parameters chosen. This example illustrates the variation in the results for a given selection of parameters, and can easily be applied to other desired scenarios.

### 4 Closing

In closing, the process of precise, targeted, shot-peening applied deep within confined interior keyways and pathways inside complex machine components is an area of ongoing

research. The approaches utilize long needle-like nozzles that induce impact which are oblique. Generally, one would like to avoid excessive normal and tangential impact forces and re-impact from the rebounding jet on secondary, unintended target, surfaces. The present work focussed on the building block of a particulate shot-peening jet, namely the oblique inelastic impact of a particle with a frictional surface. The governing equations for a general three-dimensional inelastic impact with unilateral stick-slip conditions were derived, with the objective being to determine the relationship between pre- and post-impact particle trajectory and the imparted forces on the surface. The analysis is useful to researchers interested in using particulate jets used in manufacturing, in order to reduce trial and error procedures. Current work of the author is focussed on coupling this analysis to the deformation of an impacted surface utilizing processes such as those found in papers on the finite element analysis of the response of the substrate of a shot-peened solid such as Afazov et al. [1], Bagherifard et al. [3], Elbella et al. [10] and Chen et al. [7] and Wriggers [21]. This will require the analysis of multiple bodies in simultaneous contact, such as those found in Duran [9], Pöschel and Schwager [18], Onate et al. [15,16], Rojek et al. [19], Carbonell et al. [6], Labra and Onate [12], Leonardi et al. [13], Cante et al. [5], Rojek [20], Onate et al [17], Bolinteanu et al. [4], Avci and Wriggers [2] and Zohdi [22–25].

In particular, current extensions of the present work is building on approaches found in Zohdi [22–25], which was originally motivated by many additive manufacturing technologies involving the deposition of particles onto a surface followed by selective, targeted, laser heating, such as print-based technologies. In particular, printing on flexible foundational substrates are becoming popular, with wide-ranging applications such as flexible solar cells, smart electronics and textile printing (Fathi et al. [11]). Specifically, ongoing work involves (a) the movement of the particles induced by contact with the surface and (b) particle-to-particle contact forces, which are strongly coupled together. Furthermore, this potentially involves particle thermodynamics, which primarily entails: (a) heat transfer between particles in contact by conduction and (b) subsequent thermal softening of the particles. From a computational standpoint, it is advantageous to

**Table 1** Table of post-impact trajectories and spins

$\mu_s$	$v_{c,n}(t + \delta t)$ m/s	$v_{tn}(t + \delta t)$ m/s	$\theta(t + \delta t)$ deg	$\omega_z(t + \delta t)$ rad/s
0.300	2.1651	2.0772	46.1870	-14614.1787
0.270	2.1651	2.3694	42.4193	-13152.7608
0.240	2.1651	2.6617	39.1251	-11691.3430
0.210	2.1651	2.9540	36.2385	-10229.9251
0.180	2.1651	3.2463	33.7006	-8768.5072
0.150	2.1651	3.5386	31.4602	-7307.0893
0.120	2.1651	3.8309	29.4735	-5845.6715
0.090	2.1651	4.1231	27.7039	-4384.2536
0.060	2.1651	4.4154	26.1206	-2922.8357
0.030	2.1651	4.7077	24.6975	-1461.4179
0.000	2.1651	5.0000	23.4132	0.0000

In each case there was slipping. See Fig. 4 for the nomenclature

**Table 2** Table of imparted force-impulses and translational and rotational kinetic energies, where  $W_T(t) \stackrel{\text{def}}{=} \frac{1}{2} m \mathbf{v}(t) \cdot \mathbf{v}(t)$ ,  $W_T(t + \delta t) \stackrel{\text{def}}{=} \frac{1}{2} m \mathbf{v}(t + \delta t) \cdot \mathbf{v}(t + \delta t)$ ,  $W_R(t) \stackrel{\text{def}}{=} \frac{1}{2} \bar{I} \boldsymbol{\omega}(t) \cdot \boldsymbol{\omega}(t)$ ,  $W_R(t + \delta t) \stackrel{\text{def}}{=} \frac{1}{2} \bar{I} \boldsymbol{\omega}(t + \delta t) \cdot \boldsymbol{\omega}(t + \delta t)$  and  $\frac{W_T(t) + W_R(t)}{W_T(t + \delta t) + W_R(t + \delta t)}$ . In each case there was slipping

$\mu_s$	$N \delta t$ $\mu\text{N/s}$	$f \delta t$ $\mu\text{N/s}$	$W_T(t)$ $\mu\text{J}$	$W_T(t + \delta t)$ $\mu\text{J}$	$W_R(t)$ $\mu\text{J}$	$W_R(t + \delta t)$ $\mu\text{J}$	$\frac{W_T(t) + W_R(t)}{W_T(t + \delta t) + W_R(t + \delta t)}$
0.300	39.6769	10.7128	183.2596	16.4972	0.0000	39.1395	0.3036
0.270	39.6769	9.6415	183.2596	18.8790	0.0000	31.7030	0.2760
0.240	39.6769	8.5702	183.2596	21.5739	0.0000	25.0493	0.2544
0.210	39.6769	7.4989	183.2596	24.5819	0.0000	19.1784	0.2388
0.180	39.6769	6.4277	183.2596	27.9030	0.0000	14.0902	0.2291
0.150	39.6769	5.3564	183.2596	31.5373	0.0000	9.7849	0.2255
0.120	39.6769	4.2851	183.2596	35.4846	0.0000	6.2623	0.2278
0.090	39.6769	3.2138	183.2596	39.7451	0.0000	3.5226	0.2361
0.060	39.6769	2.1426	183.2596	44.3187	0.0000	1.5656	0.2504
0.030	39.6769	1.0713	183.2596	49.2054	0.0000	0.3914	0.2706
0.000	39.6769	0.0000	183.2596	54.4052	0.0000	0.0000	0.2969

couple the various submodels comprising the overall multi-body system using iterative staggering schemes, whereby the strong multiphysics-coupled sub-models are solved iteratively within each time-step using a recursive staggering scheme, which employs temporal adaptivity to control the numerical error.

**References**

1. Afazov SM, Becker AA, Hyde TH (2012) Mathematical modeling and implementation of residual stress mapping from microscale to macroscale finite element models. *J Manuf Sci Eng* 134(2):021001–021001-11
2. Avci B, Wriggers P (2012) A DEM–FEM coupling approach for the direct numerical simulation of 3D particulate flows. *J Appl Mech* 79:010901-(1-7)
3. Bagherifard S, Giglio M, Giudici L, Guagliano M (2010). Experimental and numerical analysis of fatigue properties improvement in a titanium alloy by shot peening. In: *Proceedings of ASME*

- 49163; ASME 2010 10th Biennial conference on engineering systems design and analysis, vol 2, pp 317–322
4. Bolintineanu DS, Grest GS, Lechman JB, Pierce F, Plimpton SJ, Schunk PR (2014) Particle dynamics modeling methods for colloid suspensions. *Comput Part Mech* 1(3):321–356
5. Cante J, Davalos C, Hernandez JA, Oliver J, Jonsen P, Gustafsson G, Haggblad HA (2014) PFEM-based modeling of industrial granular flows. *Comput Part Mech* 1(1):47–70
6. Carbonell JM, Onate E, Suarez B (2010) Modeling of ground excavation with the particle finite element method. *J Eng Mech ASCE* 136:455–463
7. Chen Z, Yang F, Meguid SA (2014) Realistic finite element simulations of arc-height development in shot-peened almen strips. *J Eng Mater Technol* 136(4):041002–041002-7
8. Dirksen F, Anselmann M, Zohdi TI, Lammering R (2013) Incorporation of flexural hinge fatigue-life cycle criteria into the topological design of compliant small-scale devices. *Precis Eng* 37:531–541
9. Duran J (1997) *Sands, powders and grains. An introduction to the physics of granular matter.* Springer, New York
10. Elbella A, Fadul F, Uddanda SH, Kasarla NR (2012) Influence of shot peening parameters on process effectiveness. In: *Proceedings*

- ASME, 45196; vol 3: design, materials and manufacturing, parts A, B and C, pp 2015–2021
11. Fathi S, Dickens P, Khodabakhshi K, Gilbert M (2013) Microcrystal particles behaviour in inkjet printing of reactive nylon materials. *J Manuf Sci Eng* 135:011009. doi:[10.1115/1.4023272](https://doi.org/10.1115/1.4023272)
  12. Labra C, Onate E (2009) High-density sphere packing for discrete element method simulations. *Commun Numer Methods Eng* 25(7):837–849
  13. Leonardi A, Wittel FK, Mendoza M, Herrmann HJ (2014) Coupled DEM–LBM method for the free-surface simulation of heterogeneous suspensions. *Comput Part Mech* 1(1):3–13
  14. Lum GZ, Teo TJ, Yang G, Yeo SH, Sitti M (2014) Integrating mechanism synthesis and topological optimization technique for stiffness-oriented design of a three degrees-of-freedom flexure-based parallel mechanism. *Precis Eng* 39:125–133
  15. Onate E, Idelsohn SR, Celigueta MA, Rossi R (2008) Advances in the particle finite element method for the analysis of fluid-multibody interaction and bed erosion in free surface flows. *Comput Methods Appl Mech Eng* 197(19–20):1777–1800
  16. Onate E, Celigueta MA, Idelsohn SR, Salazar F, Surez B (2011) Possibilities of the particle finite element method for fluid-soil-structure interaction problems. *Comput Mech* 48:307–318
  17. Onate E, Celigueta MA, Latorre S, Casas G, Rossi R, Rojek J (2014) Lagrangian analysis of multiscale particulate flows with the particle finite element method. *Comput Part Mech* 1(1):85–102
  18. Pöschel T, Schwager T (2004) *Computational granular dynamics*. Springer, Berlin
  19. Rojek J, Labra C, Su O, Onate E (2012) Comparative study of different discrete element models and evaluation of equivalent micromechanical parameters. *Int J Solids Struct* 49:1497–1517. doi:[10.1016/j.ijsolstr.2012.02.032](https://doi.org/10.1016/j.ijsolstr.2012.02.032)
  20. Rojek J (2014) Discrete element thermomechanical modelling of rock cutting with valuation of tool wear. *Comput Part Mech* 1(1):71–84
  21. Wriggers P (2002) *Computational contact mechanics*. Wiley, New York
  22. Zohdi TI (2012) *Dynamics of charged particulate systems. Modeling, theory and computation*. Springer, New York
  23. Zohdi TI (2013) Numerical simulation of charged particulate cluster-droplet impact on electrified surfaces. *J Comput Phys* 233:509–526
  24. Zohdi T (2014) Embedded electromagnetically sensitive particle motion in functionalized fluids. *Comput Part Mech* 1(1):27–45
  25. Zohdi TI (2014) Rapid computation of statistically-stable particle/feature ratios for consistent substrate stresses in printed flexible electronics. *J Manuf Sci Eng ASME (MANU-14-1476)*. doi:[10.1115/1.4029327](https://doi.org/10.1115/1.4029327)